Improved Grid Synchronization Control of Doubly Fed Induction Generator Under Unbalanced Grid Voltage

Si Zhe Chen, Norbert C. Cheung, *Senior Member, IEEE*, Yun Zhang, Miao Zhang, and Xiong Min Tang

***Abstract*—An improved grid synchronization control scheme of the wind energy conversion system based on the doubly fed induction generator (DFIG) under unbalanced grid voltage is proposed in this paper. In both the positive and negative sequence models, respectively, the degrees of relevancy among rotor voltages, rotor currents, and stator voltages are calculated using the relative gain array (RGA) methodology. According to the analysis results of RGA, the main controller is designed to control positive sequence stator voltages directly with positive sequence rotor voltages, and the auxiliary controller is designed to control negative sequence stator voltages directly with negative sequence rotor voltages. Hence, the rotor current control loops are eliminated, which simplifies the structure of the controller. Simulation and hardware experimental results validate that the improved control scheme effectively controls stator voltages of the DFIG to accurately follow unbalanced grid voltage and, hence, avoids current, torque, and power impacts to both the DFIG and the grid at the time of connecting.**

***Index Terms*—Doubly fed induction generator (DFIG), grid synchronization, unbalanced grid voltage, wind energy conversion system.**

NOMENCLATURE

F	Variable representing voltage, current, and flux.
φ_+, φ_-	Phase shift for positive and negative sequence components.
u_g, u_s, u_r	Grid, stator, and rotor winding voltage.
i_r	Rotor winding current.
λ_s, λ_r	Stator and rotor flux.
$\omega_e, \omega_r, \omega_{\rm slip}$	Synchronous, rotor, and slip speed.
$\theta_e, \theta_r, \theta_{\rm slip}$	Angle of stator flux, rotor, and slip.
R_r	Rotor winding resistance.
L_m, L_r	Magnetizing and rotor self-inductance.
p_n	Number of pole pairs.
Δ	Switching control.
Superscripts	
$+, -$	Positive and negative sequence synchronous reference frames.
eq	Equivalent control.
$*$	Reference value for a controller.
Subscripts	
$+, -$	Positive and negative sequence components.
α, β	Stationary α–β axis.
d, q	Synchronous d–q axis.
g, s, r	Grid, stator, and rotor.
0	Nominal value of the parameter.

Manuscript received August 25, 2010; revised November 25, 2010 and March 6, 2011; accepted May 26, 2011. Date of publication June 27, 2011; date of current version August 19, 2011. This work was supported by the Natural Science Foundation of Guangdong Province under Grant 8351009001000002, the Science and Technology Planning Project of Guangdong Province under Grant 2009A080304011, and the "211 Project" of Guangdong Province under Grant YueFaGai 431. Paper no. TEC-00339-2010.

S. Z. Chen, Y. Zhang, M. Zhang, and X. M. Tang are with the Faculty of Automation, Guangdong University of Technology, Guangzhou 510006, China (e-mail: cszscut@126.com; yz@gdut.edu.cn; bezhangm@gdut.edu.cn; tangxiongmin@126.com).

N. C. Cheung is with the Department of Electrical Engineering, The Hong Kong Polytechnic University, Kowloon, Hong Kong (e-mail: norbert.cheung@polyu.edu.hk).

Digital Object Identifier 10.1109/TEC.2011.2158580

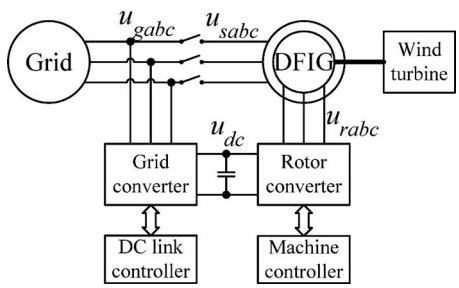

Fig. 1. WECS based on the DFIG.

I. INTRODUCTION

WIND energy generation becomes more and more popular, because of the gradual depletion of fossil energy resources and the increasingly concern for environmental pollution. The wind energy conversion system (WECS) based on the doubly fed induction generator (DFIG), of which the topology is shown in Fig. 1, is widely applied in high-power wind energy generation. As shown in Fig. 1, the stator windings of the DFIG are directly connected to the grid, and the rotor windings are connected to the grid through a back-to-back PWM converter. The WECS based on the DFIG operates at variable speed constant frequency mode, which provides a lot of advantages including maximizing the captured wind power, reducing mechanical stresses, and improving the power quality [1]. Furthermore, the power electronics converter only needs to process a portion of the generated energy, which reduces the rating and cost of the converter [2]. Hence, the WECS based on the DFIG is very suitable for high-power wind energy generation.

Two significant control issues of the DFIG are power decoupled control (or torque control) and grid synchronization control.

Stator-flux-oriented control scheme and stator-voltage-oriented control scheme have been proposed in [3] and [4], respectively, to achieve power decoupled control of the DFIG. As alternatives to aforementioned vector-oriented control schemes, direct power control scheme and direct torque control scheme have been proposed in [5] and [6], respectively, to reduce the parameter dependence and simplify the control algorithms.

Besides power decoupled control, grid synchronization control is another important issue in the application of the WECS based on the DFIG, which enables the DFIG to be connected to the power grid with minimum impacts to both the WECS and the grid. In [7], only the rotor current control loop is used for grid synchronization. The lack of voltage feedback might result in significant differences between stator and grid voltages. Cascaded control schemes are designed in [8] and [9], in which the inner loop controls rotor currents and the outer loop controls stator voltages. Hence, the differences between stator and grid voltages are eliminated. Stator voltages of the DFIG are directly controlled by rotor voltages in [10], which eliminate the rotor current control loop in cascaded control schemes. Hence, the demand on the computation power and the number of parameters for tuning can be reduced. A grid synchronization control scheme using integral variable structure control is proposed in [11], in which parametric uncertainties and external disturbances are formally included into the design procedure of a controller. Hence, the robustness of the system against parametric errors and external disturbances can be guaranteed.

The power decoupled and grid synchronization control schemes mentioned earlier are all designed under balanced grid voltage. However, WECS is usually located in rural areas with weak grid connection, in which grid voltage unbalance may arise even during normal operation. The unbalanced grid voltage may be caused by unbalanced transmission line impedance, three-phase unbalanced load, and single-phase high-power load [12].

Many improved power decoupled schemes have been proposed in [13]–[16] to eliminate torque and power pulsations of the DFIG caused by unbalanced grid voltage. A method proposed in [17] reduces required negative sequence rotor voltage by injecting additional negative sequence rotor current, which enhances positive sequence power control capabilities of the DFIG under unbalanced grid voltage. However, no research is reported at present about the grid synchronization control of the DFIG under unbalanced grid voltage, which is also important for the protections of both the WECS and the grid. If the grid voltage unbalance is not taken into account in grid synchronization control of the DFIG, the differences between stator voltages and grid voltages will become significant, which will cause large current, torque, and power impact at the time of connecting.

In this paper, an improved grid synchronization control scheme is proposed to control stator voltages of the DFIG to accurately follow unbalanced grid voltages. Different from existing grid synchronization control schemes, stator voltages and grid voltages are decomposed into positive and negative sequence components. Positive sequence stator voltages are controlled by the main controller in the positive sequence synchronous reference frame, and negative sequence stator voltages are controlled by the auxiliary controller in the negative sequence synchronous reference frame. Simulation and hardware experimental results show that the stator voltages of the DFIG are capable of following unbalanced grid voltages accurately with the proposed control scheme, which avoids current, torque, and power impacts to both the DFIG and the grid at the time of connecting.

II. Mathematical Model of DFIG Under Unbalanced Grid Voltage

The integrated mathematical model and coordinate transformation relationship of the DFIG under unbalanced grid voltage have been presented in [14]–[16]. In this section, the model of the DFIG during grid synchronization will be briefly introduced.

If the neutral point of the DFIG is not connected to the grid, all the unbalanced voltage, current, and flux vectors can be decomposed as the superposition of positive and negative sequence components as follows:

$$\begin{aligned}\vec{F}_{\alpha\beta}(t) &= \vec{F}_{\alpha\beta+}(t) + \vec{F}_{\alpha\beta-}(t) \\ &= |\vec{F}_{\alpha\beta+}|e^{j(\omega_e t+\varphi_+)} + |\vec{F}_{\alpha\beta-}|e^{j(-\omega_e t+\varphi_-)}. \quad (1)\end{aligned}$$

In the positive sequence synchronous reference frame, which rotates at synchronous speed, the positive sequence model of the DFIG during grid synchronization is

$$\vec{u}^{+}_{dqs+} = \frac{d\vec{\lambda}^{+}_{dqs+}}{dt} + j\omega_e\vec{\lambda}^{+}_{dqs+} \quad (2)$$

$$\vec{u}^{+}_{dqr+} = R_r\vec{i}^{+}_{dqr+} + \frac{d\vec{\lambda}^{+}_{dqr+}}{dt} + j\omega_{\text{slip}+}\vec{\lambda}^{+}_{dqr+} \quad (3)$$

$$\vec{\lambda}^{+}_{dqs+} = L_m\vec{i}^{+}_{dqr+} \quad (4)$$

$$\vec{\lambda}^{+}_{dqr+} = L_r\vec{i}^{+}_{dqr+} \quad (5)$$

where $\omega_{\text{slip}+} = (\omega_e - p_n\omega_r)$.

In the negative sequence synchronous reference frame, which rotates at the same speed but in contrary direction with a positive sequence synchronous reference frame, the negative model of the DFIG during grid synchronization is

$$\vec{u}^{-}_{dqs-} = \frac{d\vec{\lambda}^{-}_{dqs-}}{dt} - j\omega_e\vec{\lambda}^{-}_{dqs-} \quad (6)$$

$$\vec{u}^{-}_{dqr-} = R_r\vec{i}^{-}_{dqr-} + \frac{d\vec{\lambda}^{-}_{dqr-}}{dt} + j\omega_{\text{slip}-}\vec{\lambda}^{-}_{dqr-} \quad (7)$$

$$\vec{\lambda}^{-}_{dqs-} = L_m\vec{i}^{-}_{dqr-} \quad (8)$$

$$\vec{\lambda}^{-}_{dqr-} = L_r\vec{i}^{-}_{dqr-} \quad (9)$$

where $\omega_{\text{slip}-} = (-\omega_e - p_n\omega_r)$.

Since the grid voltage is the only quantity not affected by the operation of the DFIG during grid synchronization, the synchronous reference frame should be aligned to the grid voltage. The q-axes of the positive and negative sequence synchronous reference frames are aligned to the positive and negative sequence components of grid voltage vector, respectively, and hence the d-axes are orthogonal to respective components of

grid voltage vector, which gives

$$u^+_{qg+} = |u_{g+}| \quad u^-_{qg-} = |u_{g-}| \quad u^+_{dg+} = u^-_{dg-} = 0. \tag{10}$$

The coordinate transformations among the stationary, positive sequence synchronous, and negative sequence synchronous reference frames are

$$\begin{aligned} \vec{F}^+_{dq} &= \vec{F}_{\alpha\beta} e^{-j(\omega_e t+\varphi_+)} \qquad \vec{F}^+_{dq} = \vec{F}^-_{dq} e^{-j2\omega_e t} e^{-j(\varphi_+ -\varphi_-)} \\ \vec{F}^-_{dq} &= \vec{F}_{\alpha\beta} e^{-j(-\omega_e t+\varphi_-)} \qquad \vec{F}^-_{dq} = \vec{F}^+_{dq} e^{j2\omega_e t} e^{j(\varphi_+ -\varphi_-)}. \end{aligned} \tag{11}$$

According to the model of the DFIG under unbalanced grid voltage, two controllers are needed to regulate stator voltages to achieve the same magnitude, frequency, and phase with unbalanced grid voltages. The objective of the main controller is to regulate the positive sequence stator direct and quadrature voltages to track corresponding positive sequence grid voltages in a positive sequence synchronous reference frame, respectively. The objective of the auxiliary controller is to regulate the negative sequence stator direct and quadrature voltages to track corresponding negative sequence grid voltages in a negative sequence synchronous reference frame, respectively.

III. Main Controller Design

In order to choose appropriate input–output control pairs in the DFIG under unbalanced grid voltage, the relative gain array (RGA) methodology [18] will be used to calculate the degrees of relevance among rotor voltages, rotor currents, and stator voltages.

The RGA is calculated as the element-by-element product of the system transfer matrix and the inverse of its transposed matrix. An RGA element close to unity indicates that the input and output variables constitute a suitable pair that forms the formation of a control loop, while a small positive RGA element shows a low correlation between the input and output variables [10].

Substituting (4) into (2), and (5) into (3), and then separating the results into real and imaginary parts, the Laplace equations relating the positive sequence variables are

$$\begin{bmatrix} u^+_{ds+} \\ u^+_{qs+} \end{bmatrix} = \begin{bmatrix} L_m s & -\omega_e L_m \\ \omega_e L_m & L_m s \end{bmatrix} \begin{bmatrix} i^+_{dr+} \\ i^+_{qr+} \end{bmatrix} \tag{12}$$

$$\begin{bmatrix} u^+_{dr+} \\ u^+_{qr+} \end{bmatrix} = \begin{bmatrix} R_r + L_r s & -\omega_{\text{slip}+} L_r \\ \omega_{\text{slip}+} L_r & R_r + L_r s \end{bmatrix} \begin{bmatrix} i^+_{dr+} \\ i^+_{qr+} \end{bmatrix}. \tag{13}$$

The RGA of the matrix in (12) is

$$\begin{aligned} &\begin{bmatrix} L_m s & -\omega_e L_m \\ \omega_e L_m & L_m s \end{bmatrix} .\times \left(\begin{bmatrix} L_m s & -\omega_e L_m \\ \omega_e L_m & L_m s \end{bmatrix}^T \right)^{-1} \\ &\quad = \frac{1}{s^2 + \omega_e^2} \begin{bmatrix} s^2 & \omega_e^2 \\ \omega_e^2 & s^2 \end{bmatrix} \end{aligned} \tag{14}$$

where '.×' means element-by-element multiplication.

Since the RGA is only used to analyze the DFIG model, it is sufficient to be evaluated at zero frequency to give valid input–output pairs at steady state [18], which means that the s terms are zero. Since the values of the diagonal elements are zero and the values of the off-diagonal elements are unit in (14), the appropriate input–output control pairs in (12) should be direct rotor current to quadrature stator voltage and quadrature rotor current to direct stator voltage.

The RGA of the matrix in (13) is

$$\begin{aligned} &\begin{bmatrix} R_r + L_r s & -\omega_{\text{slip}+} L_r \\ \omega_{\text{slip}+} L_r & R_r + L_r s \end{bmatrix} \\ &\quad .\times \left(\begin{bmatrix} R_r + L_r s & -\omega_{\text{slip}+} L_r \\ \omega_{\text{slip}+} L_r & R_r + L_r s \end{bmatrix}^T \right)^{-1} \\ &\quad = \frac{1}{(R_r + L_r s)^2 + (\omega_{\text{slip}+} L_r)^2} \\ &\quad \times \begin{bmatrix} (R_r + L_r s)^2 & (\omega_{\text{slip}+} L_r)^2 \\ (\omega_{\text{slip}+} L_r)^2 & (R_r + L_r s)^2 \end{bmatrix}. \end{aligned} \tag{15}$$

If the DFIG operates at synchronous speed, values of the diagonal elements are unit and values of the off-diagonal elements are zero in (15). Hence, the appropriate input–output control pairs in (13) should be direct rotor voltage to direct rotor current and quadrature rotor voltage to quadrature rotor current. The same conclusion would be obtained if the DFIG operates at other speeds in the vicinity of synchronous speed.

According to the aforementioned model analysis, the appropriate input–output control relationship among positive sequence variables in a positive sequence synchronous reference frame is

$$\begin{cases} u^+_{dr+} \rightarrow i^+_{dr+} \rightarrow u^+_{qs+} \\ u^+_{qr+} \rightarrow i^+_{qr+} \rightarrow u^+_{ds+}. \end{cases} \tag{16}$$

According to the numeric results of (14) and (15), the diagonal terms of the matrix in (12) and the off-diagonal terms of the matrix in (13) can be regarded as disturbances. Basing on the previous analysis results and using a similar deductive process in [11], the positive sequence model of the DFIG in a positive sequence synchronous reference frame is given as

$$\begin{cases} \dfrac{du^+_{ds+}}{dt} = -\dfrac{\omega_e L_m}{L_r} u^+_{qr+} + \dfrac{\omega_e L_m R_r}{L_r} i^+_{qr+} + L_m \dfrac{d^2 i^+_{dr+}}{dt^2} \\ \qquad\qquad +\omega_e \omega_{\text{slip}+} L_m i^+_{dr+} \\ \dfrac{du^+_{qs+}}{dt} = \dfrac{\omega_e L_m}{L_r} u^+_{dr+} - \dfrac{\omega_e L_m R_r}{L_r} i^+_{dr+} + L_m \dfrac{d^2 i^+_{qr+}}{dt^2} \\ \qquad\qquad +\omega_e \omega_{\text{slip}+} L_m i^+_{qr+}. \end{cases} \tag{17}$$

The grid synchronization control scheme of the DFIG using integral variable structure control (IVSC), which has been designed and demonstrated in [11], will be adopted as the main controller in this improved control scheme. The robustness of the IVSC scheme against parametric errors and external disturbances has been validated by computer simulation and hardware experiment. In this section, the main controller based on IVSC will be introduced briefly. For a detailed design process, the reader can refer to [11].

The control objective of the main controller is to control positive sequence stator direct and quadrature voltages to track corresponding positive sequence grid voltages, respectively. Hence,

state variables should be defined as errors between positive sequence grid and stator voltages

$$\begin{cases} x_{d+} = u^{+}_{ds+} - u^{+*}_{ds+} = u^{+}_{ds+} - u^{+}_{dg+} \\ x_{q+} = u^{+*}_{qs+} - u^{+}_{qs+} = u^{+}_{qg+} - u^{+}_{qs+}. \end{cases} \tag{18}$$

Based on the aforementioned state variables, sliding surfaces of the system are designed as

$$\begin{cases} s_{d+} = x_{d+} + c\int_{-\infty}^{t} x_{d+}(z)dz_{d+} = 0 \\ s_{q+} = x_{q+} + c\int_{-\infty}^{t} x_{q+}(z)dz_{q+} = 0. \end{cases} \tag{19}$$

The outputs of the IVSC consist of equivalent controls and switching controls as follows:

$$\begin{cases} u^{+}_{qr+} = u^{eq+}_{qr+} + \Delta u^{+}_{qr+} \\ u^{+}_{dr+} = u^{eq+}_{dr+} + \Delta u^{+}_{dr+}. \end{cases} \tag{20}$$

Equivalent controls are used to control the nominal plant model, and switching controls are added to ensure desired performance despite parametric uncertainties and external disturbances.

By using the condition of the equivalent controls as $\dot{s} = 0$ [19], the equivalent controls are derived as

$$\begin{cases} u^{\mathrm{eq}+}_{qr+} = R_{r0}i^{+}_{qr+} + \omega_{\mathrm{slip}+}L_{r0}i^{+}_{dr+} + \dfrac{L_{r0}c}{\omega_e L_{m0}}x_{d+} \\ \qquad\qquad - \dfrac{L_{r0}}{\omega_e L_{m0}}\dfrac{du^{+*}_{ds+}}{dt} \\ u^{\mathrm{eq}+}_{dr+} = R_{r0}i^{+}_{dr+} - \omega_{\mathrm{slip}+}L_{r0}i^{+}_{qr+} + \dfrac{L_{r0}c}{\omega_e L_{m0}}x_{q+} \\ \qquad\qquad + \dfrac{L_{r0}}{\omega_e L_{m0}}\dfrac{du^{+*}_{qs+}}{dt}. \end{cases} \tag{21}$$

The switching controls are given as

$$\begin{cases} \Delta u^{+}_{qr+} = K_{d1+}x_{d+}\mathrm{sign}(s_{d+}x_{d+}) + K_{d2+}\mathrm{sign}(s_{d+}) \\ \Delta u^{+}_{dr+} = K_{q1+}x_{q+}\mathrm{sign}(s_{q+}x_{q+}) + K_{q2+}\mathrm{sign}(s_{q+}). \end{cases} \tag{22}$$

The constants *K* in (22) are determined by the well-known Lyapunov stability condition as

$$\begin{cases} s_{d+}\dot{s}_{d+} < 0 \\ s_{q+}\dot{s}_{q+} < 0. \end{cases} \tag{23}$$

The differential terms of stator voltage reference values in (21) will be infinite if the reference values of stator voltage are abruptly changed; hence, the rising and falling rates of input reference signals should be limited [11]. The switching actions in (22) will result in a chattering phenomenon, which can be conquered using a boundary layer solution by replacing sign functions with saturation functions in a small vicinity of the sliding surface [19].

IV. Auxiliary Controller Design

Substituting (8) into (6), and (9) into (7), and then separating the results into real and imaginary parts, the Laplace equations relating the negative sequence variables are

$$\begin{bmatrix} u^{-}_{ds-} \\ u^{-}_{qs-} \end{bmatrix} = \begin{bmatrix} L_m s & \omega_e L_m \\ -\omega_e L_m & L_m s \end{bmatrix} \begin{bmatrix} i^{-}_{dr-} \\ i^{-}_{qr-} \end{bmatrix} \tag{24}$$

$$\begin{bmatrix} u^{-}_{dr-} \\ u^{-}_{qr-} \end{bmatrix} = \begin{bmatrix} R_r + L_r s & -\omega_{\mathrm{slip}-}L_r \\ \omega_{\mathrm{slip}-}L_r & R_r + L_r s \end{bmatrix} \begin{bmatrix} i^{-}_{dr-} \\ i^{-}_{qr-} \end{bmatrix}. \tag{25}$$

The RGA of the matrix in (24) is

$$\begin{bmatrix} L_m s & \omega_e L_m \\ -\omega_e L_m & L_m s \end{bmatrix} . \times \left(\begin{bmatrix} L_m s & \omega_e L_m \\ -\omega_e L_m & L_m s \end{bmatrix}^T \right)^{-1} = \frac{1}{s^2 + \omega_e^2} \begin{bmatrix} s^2 & \omega_e^2 \\ \omega_e^2 & s^2 \end{bmatrix}. \tag{26}$$

Since values of the diagonal elements are zero and values of the off-diagonal elements are unit in (26), the appropriate input–output control pairs in (24) should be direct rotor current to quadrature stator voltage and quadrature rotor current to direct stator voltage.

The RGA of the matrix in (25) is

$$\begin{bmatrix} R_r + L_r s & -\omega_{\mathrm{slip}-}L_r \\ \omega_{\mathrm{slip}-}L_r & R_r + L_r s \end{bmatrix} \cdot \times \left(\begin{bmatrix} R_r + L_r s & -\omega_{\mathrm{slip}-}L_r \\ \omega_{\mathrm{slip}-}L_r & R_r + L_r s \end{bmatrix}^T \right)^{-1} = \frac{1}{(R_r + L_r s)^2 + (\omega_{\mathrm{slip}-}L_r)^2} \times \begin{bmatrix} (R_r + L_r s)^2 & (\omega_{\mathrm{slip}-}L_r)^2 \\ (\omega_{\mathrm{slip}-}L_r)^2 & (R_r + L_r s)^2 \end{bmatrix}. \tag{27}$$

If the DFIG operates at synchronous speed, values of the diagonal elements are 0.0009 and values of the off-diagonal elements are 0.9991 in (27). Hence, the appropriate input–output control pairs in (25) should be direct rotor voltage to quadrature rotor current and quadrature rotor voltage to direct rotor current. The same conclusion would be obtained if the DFIG operates at other speeds in the vicinity of synchronous speed.

According to the aforementioned model analysis, the appropriate input–output control relationship among the negative sequence variables in a negative sequence reference frame is

$$\begin{cases} u^{-}_{qr-} \rightarrow i^{-}_{dr-} \rightarrow u^{-}_{qs-} \\ u^{-}_{dr-} \rightarrow i^{-}_{qr-} \rightarrow u^{-}_{ds-}. \end{cases} \tag{28}$$

Comparing (16) with (28), it is noticed that their input–output control pairs among rotor voltages and rotor currents are different. In a positive sequence model, direct rotor current is controlled by direct rotor voltage and quadrature rotor current is controlled by quadrature rotor voltage. However, in a negative sequence model, direct rotor current is controlled by quadrature rotor voltage and quadrature rotor current is controlled by direct rotor voltage.

Referring to (15) and (27) can understand the reason. Since the DFIG operates in the vicinity of synchronous speed, the negative sequence slip speed is much larger than the positive sequence slip speed. Hence, values of off-diagonal elements are close to zero in (15) but close to unit in (27), which leads to different weight of the cross-coupling terms in (13) and (25).

According to the numeric results of (26), the diagonal terms of the matrix in (24) can be regarded as disturbances and neglected,

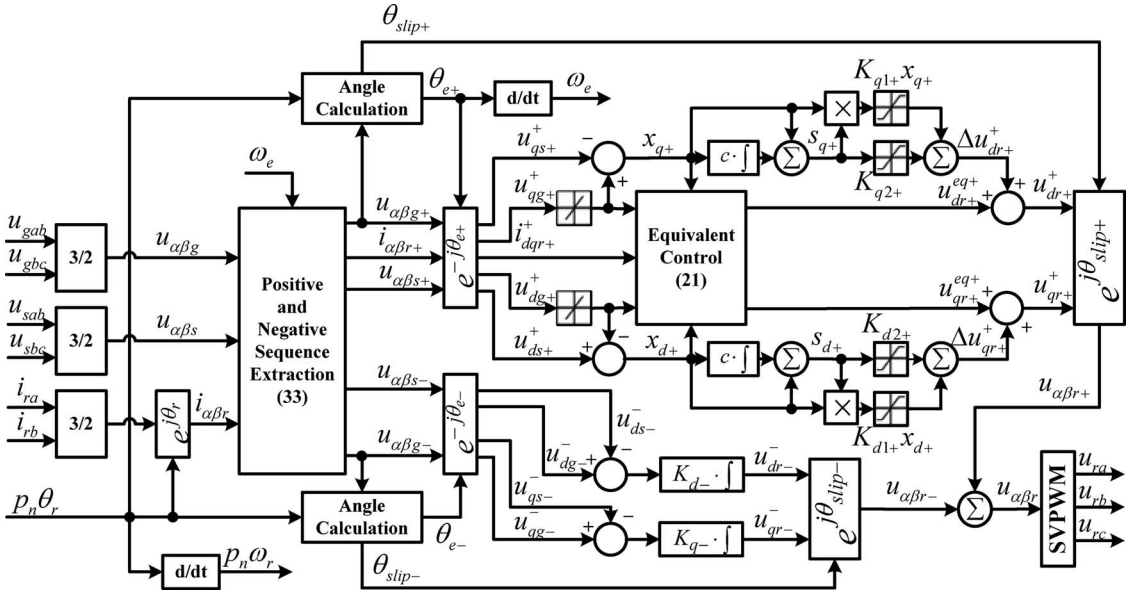

Fig. 2. Block diagram of the improved grid synchronization control scheme of the DFIG under unbalanced grid voltage.

which gives

$$\begin{bmatrix} u_{ds-}^{-} \\ u_{qs-}^{-} \end{bmatrix} = \begin{bmatrix} 0 & \omega_e L_m \\ -\omega_e L_m & 0 \end{bmatrix} \begin{bmatrix} i_{dr-}^{-} \\ i_{qr-}^{-} \end{bmatrix}. \tag{29}$$

According to the numeric results of (27), the diagonal terms of the matrix in (25) can be regarded as disturbances and neglected, which gives

$$\begin{bmatrix} u_{dr-}^{-} \\ u_{qr-}^{-} \end{bmatrix} = \begin{bmatrix} 0 & -\omega_{\text{slip}-} L_r \\ \omega_{\text{slip}-} L_r & 0 \end{bmatrix} \begin{bmatrix} i_{dr-}^{-} \\ i_{qr-}^{-} \end{bmatrix}. \tag{30}$$

Substituting (30) into (29) and rearranging gives

$$\begin{bmatrix} u_{ds-}^{-} \\ u_{qs-}^{-} \end{bmatrix} = -\frac{\omega_e L_m}{\omega_{\text{slip}-} L_r} \begin{bmatrix} u_{dr-}^{-} \\ u_{qr-}^{-} \end{bmatrix}. \tag{31}$$

Because there are no transient terms in (31), only pure integral controllers shown as (32) are adequate to achieve first-order dynamic responses in a closed-loop system

$$\begin{cases} u_{dr-}^{-} = K_{d-} \int (u_{dg-}^{-} - u_{ds-}^{-}) dt \\ u_{qr-}^{-} = K_{q-} \int (u_{qg-}^{-} - u_{qs-}^{-}) dt. \end{cases} \tag{32}$$

V. System Implementation

Integrating the main controller with the auxiliary controller gets improved grid synchronization control scheme of the DFIG under unbalanced grid voltage, the block diagram of which is shown in Fig. 2.

The proposed control scheme requires fast and accurate decomposition of positive and negative sequence components. There are several optional methods. Xu [16] adopts filters to bypass dc components and suppress double-frequency components in positive and negative sequence synchronous rotating reference frames, respectively. Weng *et al.* [20] propose a method based on cross-coupled phase-lock-loop filter to extract magnitude, frequency, and phase of positive and negative sequence components. In [14], positive and negative sequence components are calculated by adding or subtracting the present real-time signal with the signal delayed for a quarter of period in the stationary α–β reference frame. The extraction method proposed in [14] is adopted in this research, and the extraction algorithm is given as

$$\begin{cases} F_{\alpha+}(t) = \dfrac{1}{2}\left[F_\alpha(t) - F_\beta\left(t - \dfrac{\pi}{2\omega_e}\right)\right] \\ F_{\beta+}(t) = \dfrac{1}{2}\left[F_\beta(t) + F_\alpha\left(t - \dfrac{\pi}{2\omega_e}\right)\right] \\ F_{\alpha-}(t) = \dfrac{1}{2}\left[F_\alpha(t) + F_\beta\left(t - \dfrac{\pi}{2\omega_e}\right)\right] \\ F_{\beta-}(t) = \dfrac{1}{2}\left[F_\beta(t) - F_\alpha\left(t - \dfrac{\pi}{2\omega_e}\right)\right]. \end{cases} \tag{33}$$

In Fig. 2, the rotor phase angle θ_r is obtained using a rotary encoder. Synchronous speed ω_e is the derivation of θ_{e+}, in which θ_{e+} is calculated using positive sequence grid voltage in the stationary α–β reference frame.

VI. Simulation Results

The improved grid synchronization control scheme of the DFIG under unbalanced grid voltage is simulated with MATLAB/Simulink. The rotor converter is modeled as a voltage source to simulate the state-averaged operation of the converter for saving simulation time. The parameters of the DFIG are shown in the Appendix. The changing rates of the positive sequence stator quadrature voltage and direct voltage reference value are limited at ± 5000 and ± 500 V/s, respectively. The value of sliding surface coefficient c is chosen as 80. The constants in (22) are chosen as $K_{d1+} = 0.04$, $K_{d2+} = 37.23$, $K_{q1+} = 0.04$, and $K_{q2+} = 28.87$. The constants of the integral controllers in (32) are chosen as $K_{d-} = K_{q-} = 25$.

A conventional cascaded PI control scheme is also simulated for comparison, in which stator and grid voltages are not decomposed into positive and negative sequence components and the

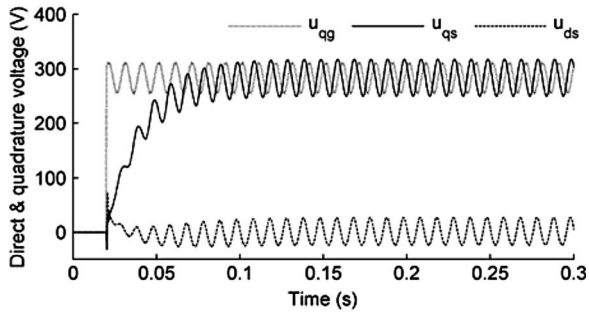

Fig. 3. Grid, stator direct, and quadrature voltages with a conventional control scheme.

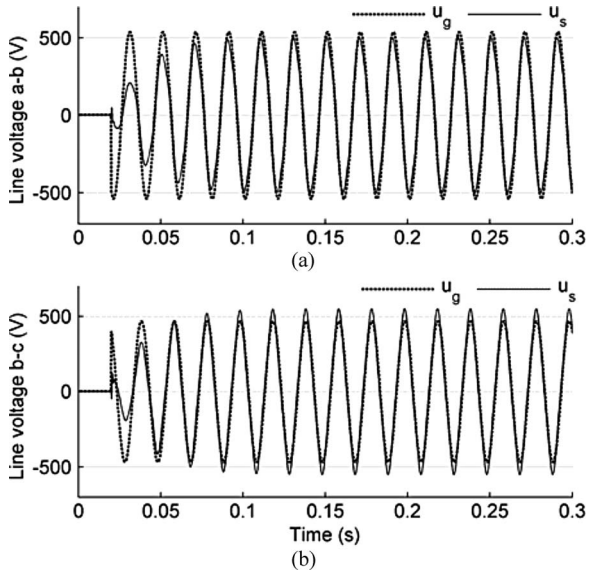

Fig. 4. Grid and stator line voltages with a conventional control scheme.

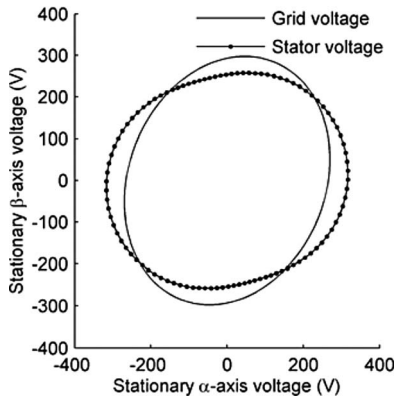

Fig. 5. Grid and stator voltage vectors at steady state with a conventional control scheme.

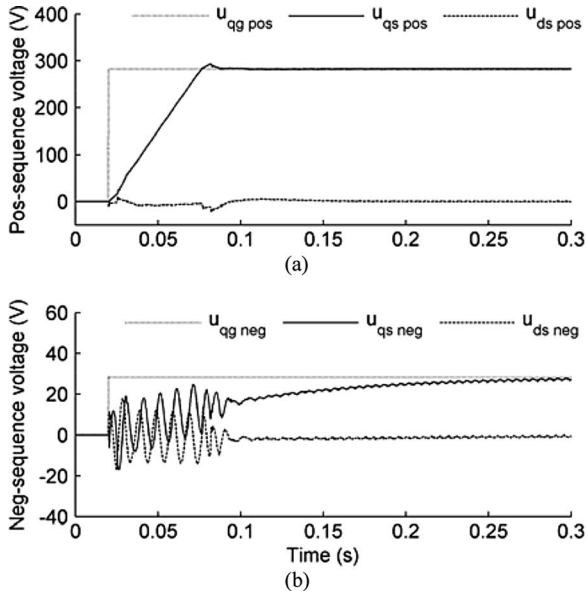

Fig. 6. Grid, stator direct, and quadrature voltages with the improved control scheme.

controller is designed only in the synchronous reference frame. The inner loop controllers are tuned to have a close-loop time constant of 0.002 s, and the outer loop controllers are tuned to have a close-loop time constant of 0.02 s.

Magnitudes of A phase and B phase voltages are kept at the rated value and the magnitude of C phase voltage is reduced to provide a three-phase unbalanced grid voltage. The ratio of negative sequence voltage to positive sequence voltage is 10%.

The grid voltage is applied at time equal to 0.02 s. Fig. 3 shows the grid quadrature voltage, stator direct voltage, and quadrature voltage of the DFIG in the synchronous reference frame when a conventional control scheme is used. Fig. 4(a) shows grid and stator line voltages between phase A and phase B, and Fig. 4(b) shows grid and stator line voltages between phase B and phase C. Fig. 5 shows the grid and stator voltage vectors at stationary reference frame during steady state.

In Fig. 3, vectors of positive sequence voltage components, which rotate at the same speed and same direction with a synchronous reference frame, form dc components. Vectors of negative sequence voltage components, which rotate at the same speed but in contrary direction with a synchronous reference frame, form 100 Hz ripples. Figs. 3–5 show that the conventional control scheme designed only in a synchronous reference frame cannot control stator voltages to accurately follow unbalanced grid voltages, which will cause current, torque, and power impact to both the DFIG and the grid at the time of connecting.

Figs. 6–8 show simulation results of the improved grid synchronization control scheme. In Fig. 6(a), positive sequence stator voltages accurately follow positive sequence grid voltages with the main controller in a positive sequence synchronous reference frame. In Fig. 6(b), negative sequence stator voltages follow negative sequence grid voltages with the auxiliary controller in a negative sequence synchronous reference frame.

To simplify the control algorithm, many s terms, of which influences on grid synchronization control during steady state are negligible according to RGA calculation results, are neglected in the design of an auxiliary controller, and hence transient responses of negative sequence stator voltages in Fig. 6 (b) are not good enough. However, amplitudes of transient oscillations in negative sequence stator voltages are very small with respect to the amplitude of positive sequence stator voltage. Hence, the influence of transient oscillations in negative sequence stator

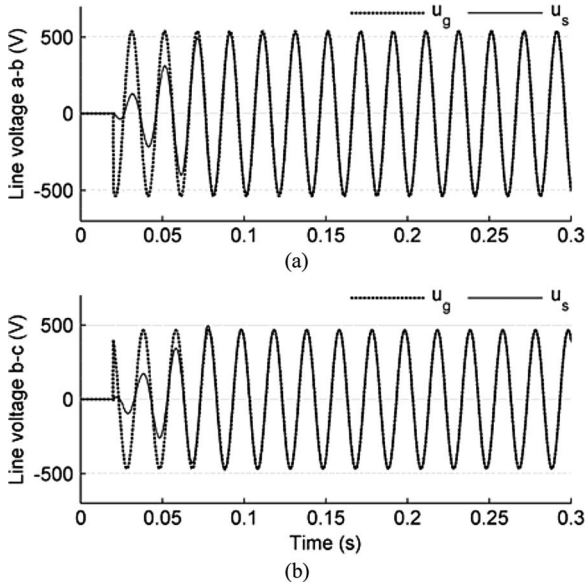

Fig. 7. Grid and stator line voltages with the improved control scheme.

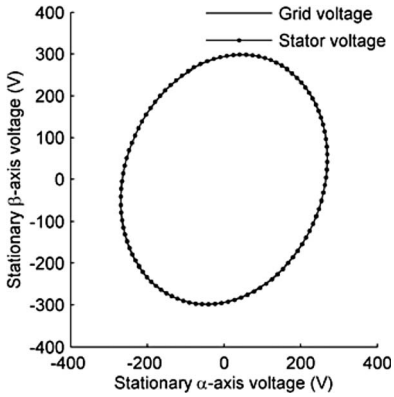

Fig. 8. Grid and stator voltage vectors at steady state with the improved control scheme.

voltage is hard to be observed in Fig. 7, and it will not degrade the whole control performance.

Figs. 6–8 show that the improved control scheme can effectively control stator voltages of the DFIG to accurately follow unbalanced grid voltages, which will reduce the impact at the time of connecting. The corresponding rotor speed is 1600 r/min (supersynchronous). Similar simulation results are obtained for other speeds within $\pm 20\%$ of the synchronous speed.

After stator voltages of the DFIG reached steady state, stator windings are connected to the grid at 0.42 s, and then the integral sliding mode direct torque control scheme proposed in [22] is adopted to eliminate torque and power pulsations. Fig. 9 shows stator and rotor A-phase current of both control schemes, and Fig. 10 shows torque, reactive power, and active power. If a conventional grid synchronization control scheme is used, transient impacts of stator and rotor currents after connecting reach 4.35 and 20.74 A, respectively, and transient impacts of torque, reactive power, and active power reach -13.12 Nm, -1.45 kVar, and -1.69 kW, respectively. The transient rotor current exceeds the rotor current ratings of the machine and the rotor converter.

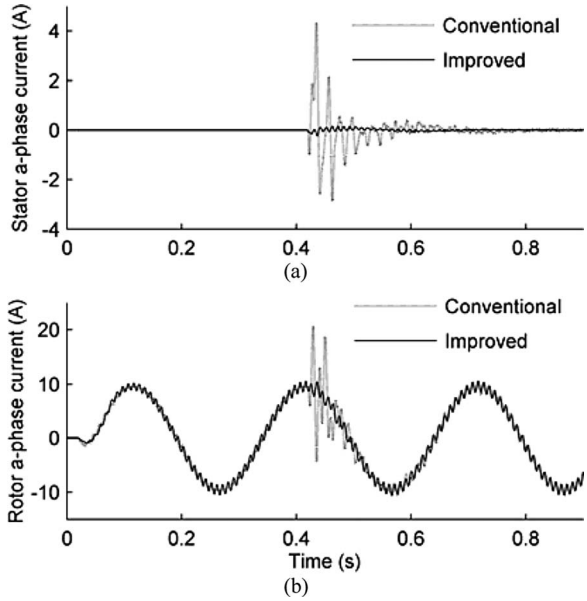

Fig. 9. Comparison of current transients between two control schemes.

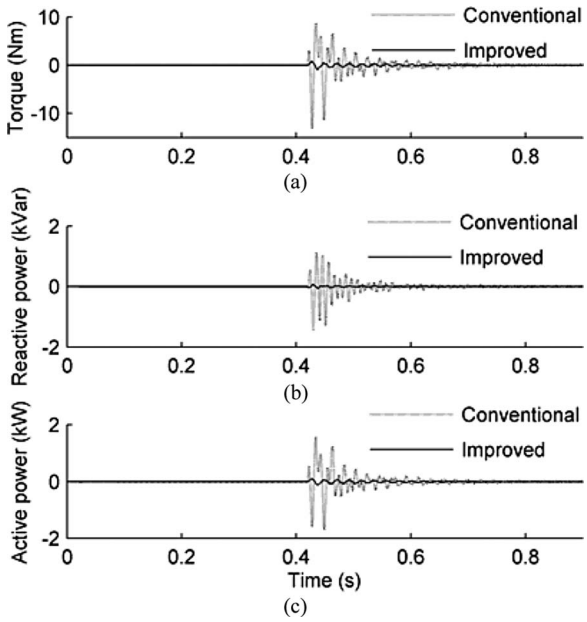

Fig. 10. Comparison of torque and power transients between two control schemes.

Transient impacts of current, torque, and power are greatly reduced by the improved grid synchronization control scheme. Hence, the improved scheme effectively protects power convertor, generator, and mechanical parts, and causes very smaller power impacts to the grid.

The improved control scheme is equally effective in voltage unbalance caused by phase angle displacement. Magnitudes of A, B, and C phase voltages are kept at the rated value, while initial phase angles of A, B and C phase voltages are set at 0°, -120°, and -223°, respectively, to produce 10% voltage unbalance factor. Simulation results of the improved control scheme under phase angle unbalance, with the rotor speed of

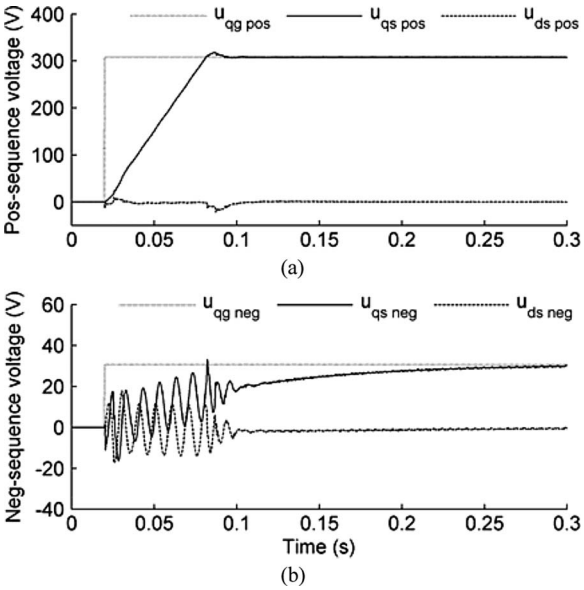

Fig. 11. Grid, stator direct, and quadrature voltages under phase angle unbalance.

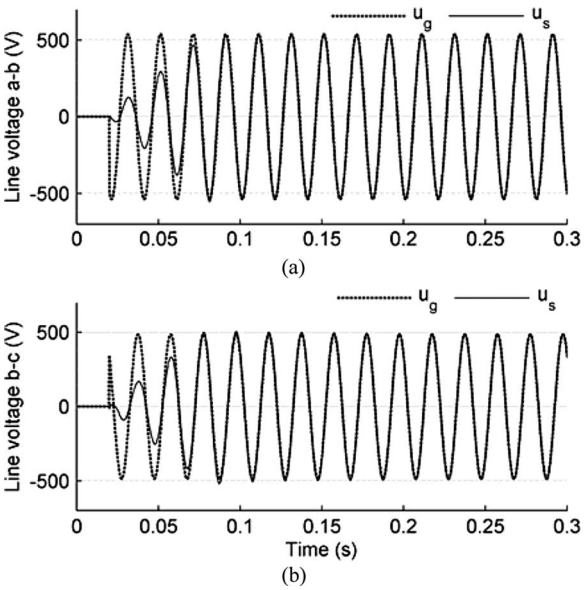

Fig. 12. Grid and stator line voltages under phase angle unbalance.

1400 r/min (sub-synchronous), are shown in Figs. 11–13. The simulation results are very similar for other speeds within $\pm 20\%$ of the synchronous speed.

Finally, sensitivity studies of the improved control scheme on grid frequency are carried out. Since the synchronous speed ω_e used in the control algorithm is calculated from grid voltage rather than fixed, the performance of a control scheme is not influenced by grid frequency error. Figs. 14–17 show simulation results when the grid frequency is 48 and 52 Hz, respectively.

VII. Hardware Experimental Results

Fig. 18 shows the configuration of the hardware experimental system. The rotor shaft of the DFIG is mechanically coupled

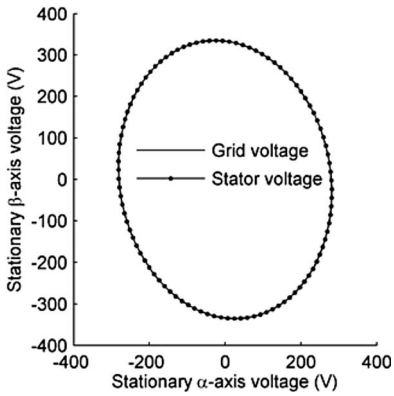

Fig. 13. Grid and stator voltage vectors at steady state under phase angle unbalance.

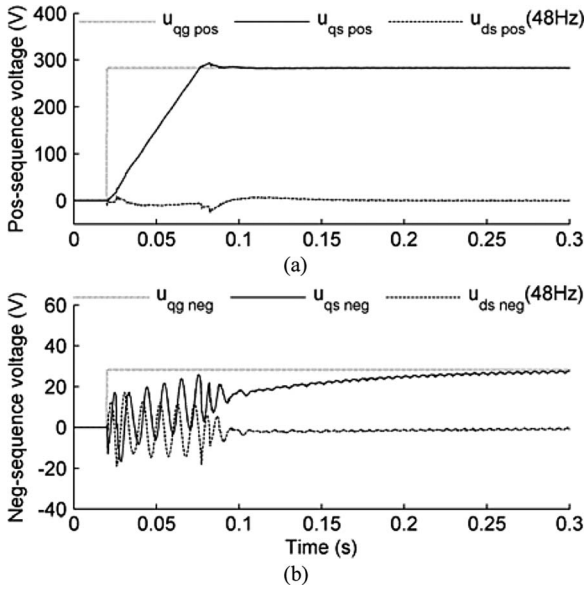

Fig. 14. Grid, stator direct, and quadrature voltages when the grid frequency is 48 Hz.

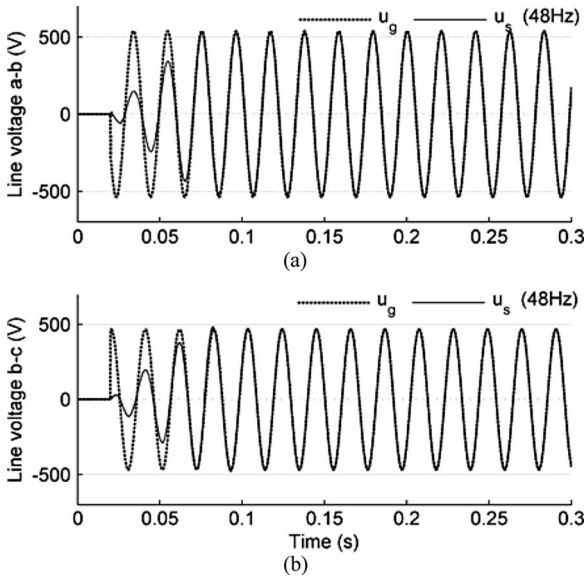

Fig. 15. Grid and stator line voltages when the grid frequency is 48 Hz.

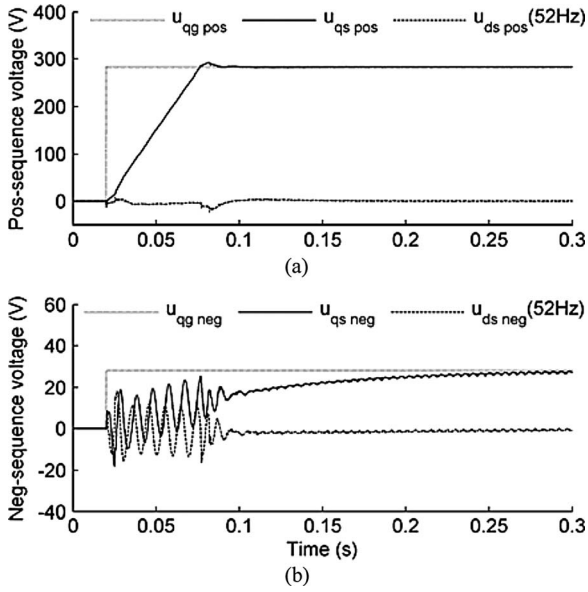

Fig. 16. Grid, stator direct, and quadrature voltages when the grid frequency is 52 Hz.

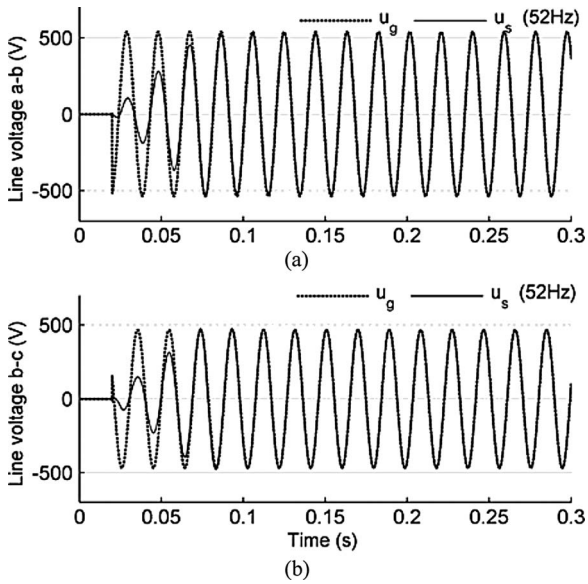

Fig. 17. Grid and stator line voltages when the grid frequency is 52 Hz.

with a separately excited dc motor. The rotor-side converter is an integrated power module (IPM)-based inverter controlling the voltage applied to the rotor winding of the DFIG. The dSpace DS1103 is a prototyping card installed in a personal computer (PC). It acquires grid line voltage, stator line voltages, rotor currents, rotor position, and dc source voltage at a rate of 5 kHz, and processes them with the control algorithm. The card then generates 10-kHz SVPWM switching signal for the rotor-side convertor control. The operating conditions and signals are displayed and stored in the PC in which the prototyping card is installed.

In the experimental system, the magnitude of C-phase grid voltage is reduced by an autotransformer to provide a three-phase unbalanced grid voltage. The ratio of negative sequence

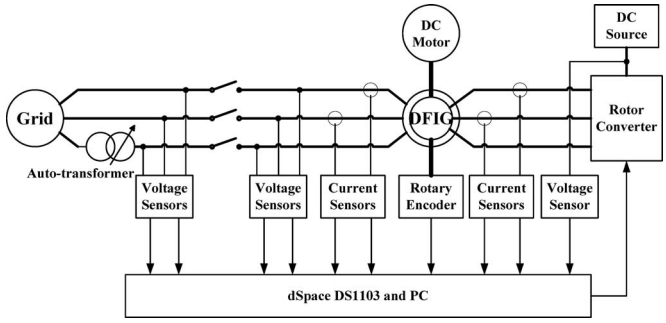

Fig. 18. Configuration of the experimental system.

to positive sequence voltage is 10%. The parameters of the DFIG are shown in the Appendix. All controller constants and variables in experiments are the same as those in simulations.

In an integrated grid-connected DIFG wind turbine, a rotor converter is connected to the grid through a dc link and grid-side convertor. The unbalanced grid voltage will cause dc voltage ripples, which will influence the rotor convertor. Hence, the dc voltage ripples should be eliminated by the grid-side PWM convertor. In [21], a dual current control scheme for a PWM converter under unbalanced grid voltage is proposed to eliminate dc voltage ripples, and hence, constant dc voltage is achieved. A grid-side convertor control scheme to eliminate dc voltage ripples in a grid-connected DFIG under unbalanced grid voltage is proposed in [14].

Since dc voltage ripples can be effectively eliminated by the existing control scheme of grid-side convertor, this paper focus on the control of a rotor convertor, and a bidirectional dc power source is adopted to replace the grid-side converter in an experimental system. In addition, considering that the dc source voltage may fluctuate, the duty cycles of a rotor converter are calculated using the dc voltage measured by a voltage sensor.

The grid voltage is applied at time equal to 0.02 s. Fig. 19 shows the grid quadrature voltage, stator direct voltage, and quadrature voltage of the DFIG in a synchronous reference frame with a conventional control scheme. Fig. 20 shows grid and stator line voltages. Fig. 21 shows grid and stator voltage vectors at stationary reference frame during steady state. In Fig. 19, dc components are formed by the vectors of positive sequence voltage components, while 100 Hz ripples are formed by the vectors of negative sequence voltage components. Figs. 19–21 show that a conventional control scheme designed only in a synchronous reference frame cannot control stator voltages to accurately follow unbalanced grid voltages, which will cause impacts to both the DFIG and the grid at connecting time.

The hardware experimental results of the improved grid synchronization control scheme are shown in Figs. 22–24. In Fig. 22, positive sequence stator voltages are controlled to accurately follow positive sequence grid voltages in a positive sequence synchronous reference frame by the main controller, and negative sequence stator voltages are controlled to follow negative sequence grid voltages in the negative sequence synchronous reference frame by the auxiliary controller. Fig. 23 shows the grid and stator line voltages. Fig. 24 shows the grid

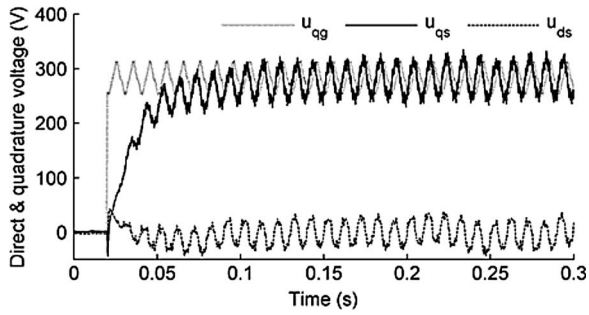

Fig. 19. Experimental grid, stator direct, and quadrature voltages with a conventional control scheme.

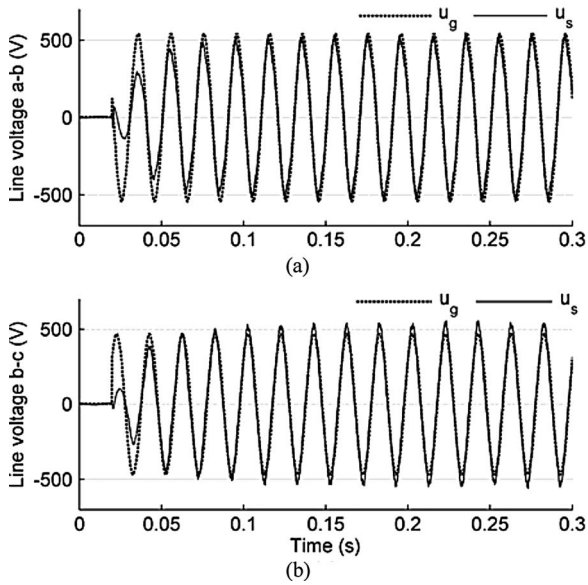

Fig. 20. Experimental grid and stator line voltages with a conventional control scheme.

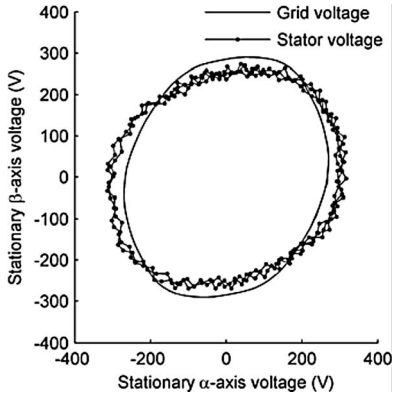

Fig. 21. Experimental grid and stator voltage vectors with a conventional control scheme.

and stator voltage vectors at stationary reference frame during steady state. Figs. 22–24 show that the improved control scheme can effectively control stator voltages of the DFIG to accurately follow unbalanced grid voltage, which will reduce the impacts at the time of connecting. Although experimental results when the rotor rotary speed is near 1400 r/min (subsynchronous) are

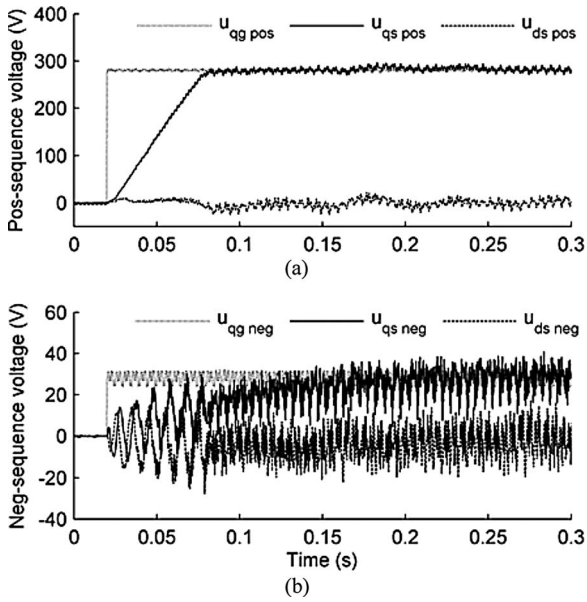

Fig. 22. Experimental grid, stator direct, and quadrature voltages with the improved control scheme.

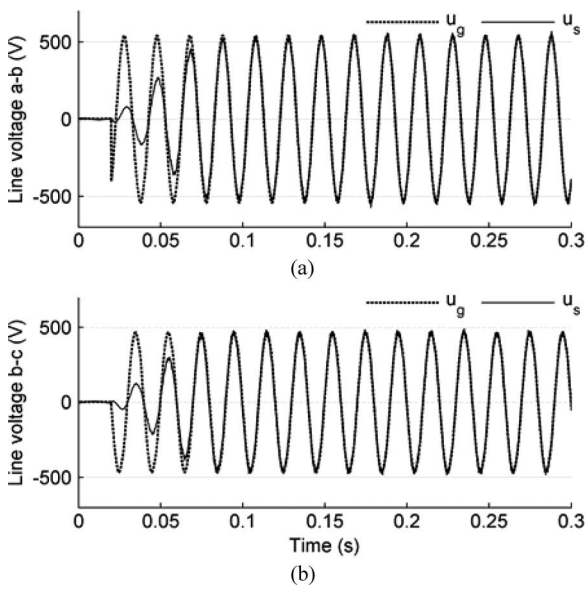

Fig. 23. Experimental grid and stator line voltages with the improved control scheme.

shown, experimental results are very similar for other speeds within ±20% of the synchronous speed.

After stator voltages of the DFIG reached steady state, stator windings are directly connected to the grid through the contactor between the stator and the grid at 0.5 s, and then the integral sliding mode direct torque control scheme proposed in [22] is adopted to eliminate torque and power pulsations. The current, torque, and power transients of the improved control scheme are shown in Figs. 25 and 26. It verifies that the improved control scheme causes very small impacts to the grid and, hence, minimizes the stress on the power convertor, generator, and mechanical parts in the transient.

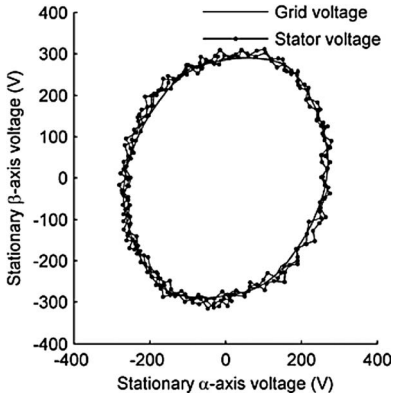

Fig. 24. Experimental grid and stator voltage vectors with the improved scheme.

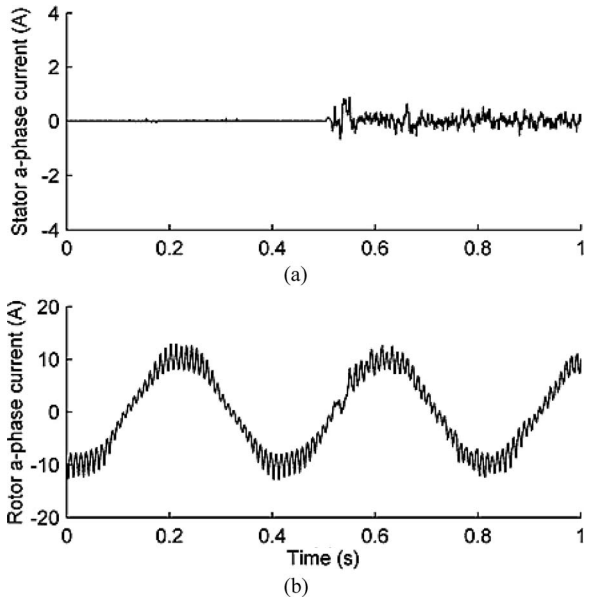

Fig. 25. Experimental current transients with the improved scheme.

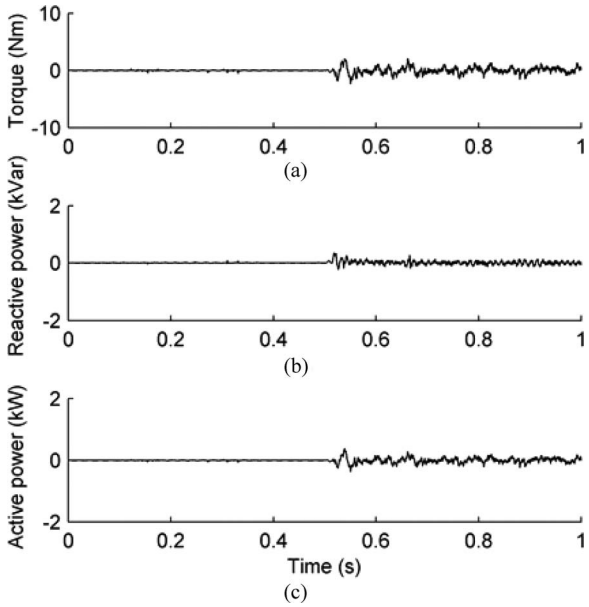

Fig. 26. Experimental torque and power transients with the improved scheme.

VIII. Conclusion

This paper proposes an improved grid synchronization control scheme of the DFIG under unbalanced grid voltage. The improved control scheme includes a main controller and an auxiliary controller. The main controller controls positive sequence stator voltages to follow positive sequence grid voltages, and the auxiliary controller controls negative sequence stator voltages to follow negative sequence grid voltages.

The degrees of relevance among rotor voltages, rotor currents, and stator voltages are calculated by the RGA methodology. According to the analysis results of the RGA, the direct control relationships among stator voltages and rotor voltages are developed, which eliminates the rotor current control loops and simplifies the structure of the controller.

Simulation and hardware experimental results validate that the improved control scheme effectively controls stator voltages of the DFIG to accurately follow unbalanced grid voltage and, hence, avoids current, torque, and power impacts to both the DFIG and the grid at the time of connecting.

Appendix

Machine parameters:

1) Stator rated voltage: 380 V.
2) Stator rated current: 4.5 A.
3) Rotor rated voltage: 120 V.
4) Rotor rated current: 10 A.
5) Rated power: 1.8 kW.
6) Operating frequency: 50 Hz.
7) Synchronous speed: 1500 r/min.
8) Magnetizing inductance (referred to the stator): 0.2987 H.
9) Rotor leakage inductance (referred to the stator): 0.0186 H.
10) Stator leakage inductance: 0.0186 H.
11) Rotor winding resistance (referred to the stator): 5.8985 Ω.
12) Stator winding resistance: 2.6596 Ω.
13) Stator-to-rotor turn ratio: 3.1667.

Acknowledgment

The authors gratefully acknowledge the technical support and advices of K. C. Wong and K. F. Wong.

References

[1] L. Y. Xu and W. Cheng, "Torque and reactive power control of a doubly fed induction machine by position sensorless scheme," *IEEE Trans. Ind. Appl.*, vol. 31, no. 3, pp. 636–642, Jun. 1995.

[2] A. Petersson, L. Harnefors, and T. Thiringer, "Evaluation of current control methods for wind turbines using doubly-fed induction machines," *IEEE Trans. Power Electron.*, vol. 20, no. 1, pp. 227–235, Jan. 2005.

[3] R. Pena, J. C. Clare, and G. M. Asher, "Doubly fed induction generator using back-to-back PWM converters and its application to variable-speed wind-energy generation," *IEE Proc. Elect. Power Appl.*, vol. 143, no. 3, pp. 231–241, May 1996.

[4] S. Muller, M. Deicke, and R. W. De Doncker, "Doubly fed induction generator systems for wind turbines," *IEEE Ind. Appl. Mag.*, vol. 17, no. 1, pp. 26–33, Jun. 2002.

[5] L. Xu and P. Cartwright, "Direct active and reactive power control of DFIG for wind energy generation," *IEEE Trans. Energy Convers.*, vol. 21, no. 3, pp. 750–758, Sep. 2006.
[6] S. Arnalte, J. C. Burgos, and J. L. Rodríguez-Amenedo, "Direct torque control of a doubly-fed induction generator for variable speed wind turbines," *Elect. Power Compon. Syst.*, vol. 30, no. 2, pp. 199–216, Feb. 2002.
[7] G. F. Yuan, J. Y. Chai, and Y. D. Li, "Vector control and synchronization of doubly fed induction wind generator system," in *Proc. 2004 Int. Power Electron. Motion Control Conf.*, pp. 886–890.
[8] L. Morel, H. Godfroid, A. Mirzaian, and J. M. Kauffmann, "Double-fed induction machine: converter optimisation and field oriented control without position sensor," *IEE Proc. Elect. Power Appl.*, vol. 145, no. 4, pp. 360–368, Jul. 1998.
[9] J. Park, K. Lee, and D. Kim, "Control method of a doubly-fed induction generator with automatic grid synchronization," in *Proc. 2006 IEEE Ind. Electron. Conf.*, pp. 4254–4259.
[10] K. C. Wong, S. L. Ho, and K. W. E. Cheng, "Direct voltage control for grid synchronization of doubly-fed induction generators," *Elect. Power Compon. Syst.*, vol. 36, no. 9, pp. 960–976, Sep. 2008.
[11] S. Z. Chen, N. C. Cheung, K. C. Wong, and J. Wu, "Grid synchronization of doubly-fed induction generator using integral variable structure control," *IEEE Trans. Energy Convers.*, vol. 24, no. 4, pp. 875–883, Dec. 2009.
[12] E. Muljadi, D. Yildirim, and T. Batan, "Understanding the unbalanced-voltage problem in wind turbine generation," in *Proc. 1999 Int. Ind. Appl. Conf.*, pp. 1359–1365.
[13] T. A. Brekken and N. Mohan, "Control of a doubly fed induction wind generator under unbalanced grid voltage conditions," *IEEE Trans. Energy Convers.*, vol. 22, no. 1, pp. 129–135, Mar. 2007.
[14] Y. Zhou, P. Bauer, J. A. Ferreira, and J. Pierik, "Operation of grid-connected DFIG under unbalanced grid voltage condition," *IEEE Trans. Energy Convers.*, vol. 24, no. 1, pp. 240–246, Mar. 2009.
[15] D. Santos-Martin, J. L. Rodriguez-Amenedo, and S. Arnalte, "Direct power control applied to doubly fed induction generator under unbalanced grid voltage conditions," *IEEE Trans. Power Electron.*, vol. 23, no. 5, pp. 2328–2336, Sep. 2008.
[16] L. Xu, "Coordinated control of DFIG's rotor and grid side converters during network unbalance," *IEEE Trans. Power Electron.*, vol. 23, no. 3, pp. 1041–1049, May 2008.
[17] H. Q. Weng, R. A. Seymour, J. D. D'Atre, A. M. Ritter, X. M. Yuan, R. C. Dai, and R. W. Delmerico, "Method, apparatus and computer program product for injecting current," U.S. Patent 7 423 412, Sep. 9, 2008.
[18] P. Albertos and A. Sala, *Multivariable Control Systems*. London: Springer-Verlag, 2004, pp. 129–136.
[19] V. I. Utkin, J. Güldner, and J. X. Shi, *Sliding Mode Control in Electromechanical Systems*, Florida: CRC Press, 1999, pp. 115–130.
[20] H. Q. Weng, J. D. D'Atre, R. A. Seymour, A. M. Ritter, X. M. Yuan, R. C. Dai, and R. W. Delmerico, "Apparatus, method and computer program product for tracking information in an electric grid," U.S. Patent 7 456 695, Nov. 25, 2008.
[21] H. S. Song and K. Nam, "Dual current control scheme for PWM converter under unbalanced input voltage conditions," *IEEE Trans. Ind. Electron.*, vol. 46, no. 5, pp. 953–959, Oct. 1999.
[22] S. Z. Chen, N. C. Cheung, K. C. Wong, and J. Wu, "Integral sliding mode direct torque control of doubly-fed induction generators under unbalanced grid voltage," *IEEE Trans. Energy Convers.*, vol. 25, no. 2, pp. 356–368, Jun. 2010.

Si Zhe Chen was born in Shantou, Guangdong, China, in 1981. He received the B.Sc. and Ph.D. degrees from the South China University of Technology, Guangzhou, China, in 2005 and 2010, respectively.

He is currently with the Faculty of Automation, Guangdong University of Technology, Guangzhou, China. His main research interest includes the control and power electronics technology in renewable energy.

Norbert C. Cheung (S'85–M'91–SM'05) received the B.Sc. degree from the University of London, London, U.K., in 1981, the M.Sc. degree from the University of Hong Kong, Pokfulam, Hong Kong, in 1987, and the Ph.D. degree from the University of New South Wales, Kensington, NSW, Australia, in 1995.

He is currently with the Department of Electrical Engineering, The Hong Kong Polytechnic University, Kowloon, Hong Kong. His research interests include motion control and power electronic drives.

Yun Zhang received the B.Sc. and M.Sc. degrees both from the Hunan University, Changsha, China, in 1982 and 1986, respectively, and the Ph.D. degree from the South China University of Technology, Guangzhou, China, in 1997.

He is currently a Professor and Doctoral Supervisor of the Faculty of Automation, Guangdong University of Technology, Guangzhou, China. His research interests include intelligent control, complex control network, and renewable energy generation.

Miao Zhang received the B.Sc. degree from the Soochow University, Soochow, China, in 1988, the M.Sc. degree from the Guangdong University of Technology, Guangzhou, China, in 1994, and the Ph.D. degree from the South China University of Technology, Guangzhou, China, in 2004.

He is currently a Professor of the Faculty of Automation, Guangdong University of Technology, Guangzhou, China. His research interests include power electronics technology in renewable energy generation.

Xiong Min Tang received the B.Sc., M.Sc., and Ph.D. degrees all from the Hunan University, Changsha, China, in 1999, 2004, and 2007, respectively.

He is currently with Faculty of Automation, Guangdong University of Technology, Guangzhou, China. His research interests include power electronics technology.